Nano-groove and 3D fabrication by controlled avalanche using femtosecond laser pulses

Ričardas Buividas,[1,2,4] **Sima Rekštytė,**[3] **Mangirdas Malinauskas,**[3] **and Saulius Juodkazis**[1,2,*]

[1]*Centre for Micro-Photonics, Faculty of Engineering and Industrial Sciences, Swinburne University of Technology, Hawthorn, VIC 3122, Australia*
[2]*The Australian National Fabrication Facility - ANFF, Victoria node, Faculty of Engineering and Industrial Sciences, Swinburne University of Technology, Hawthorn, VIC, 3122, Australia*
[3]*Laser Research Center, Department of Quantum Electronics, Physics Faculty, Vilnius University, Saulėtekio Ave. 9, bldg. III, LT-10222, Vilnius, Lithuania*
[4]*rbuividas@swin.edu.au*
[*]*Corresponding author: sjuodkazis@swin.edu.au*

Abstract: We report fabrication of sub-100 nm resolution structures by ablation on the surface of sapphire using femtosecond laser pulses. A single 50-70 nm wide groove was recorded by laser ablation via a controlled ripple formation on the surface. Ripples are created by breakdown due to a sphere-to-plane formation of an ionisation below surface in a similar way as the bulk ripples. Different thresholds for the ripples formed parallel and perpendicular to direction of the laser scan were observed. In a sol-gel photo-polymer SZ2080 and thermo-polymer polydimethylsiloxane, free-standing 3D structures were formed without use of two-photon absorbing photo-sensitizers. Both cases of the surface and bulk structuring were achieved via a controlled avalanche, which dominated ionisation of materials.

OCIS codes: (140.3390) Laser materials processing; (220.4000) Microstructure fabrication; (350.3850) Materials processing; (160.1245) Artificially engineered materials.

References and links

1. S. Maruo and K. Ikuta, "Three-dimensional microfabrication by use of single-photon-absorbed polymerization," Appl. Phys. Lett. **76**, 2656–2658 (2000).
2. C.Y. Liao, M. Bouriauand, P. L. Baldeck, J.-C. Léon, C. Masclet, and T.-T. Chung, "Two-dimensional slicing method to speed up the fabrication of microobjects based on two-photon polymerization," Appl. Phys. Lett. **91**, 033108 (2007).
3. M. Thiel, J. Fischer, G. von Freymann, and M. Wegener, "Direct laser writing of three-dimensional submicron structures using a continuous-wave laser at 532 nm," Appl. Phys. Lett. **97**, 221102 (2010).
4. M. Malinauskas, P. Danilevicius, and S. Juodkazis, "Three-dimensional micro-/nano-structuring via direct write polymerization with picosecond laser pulses," Opt. Express **19**, 5602–5610 (2011).
5. S. Maruo, O. Nakamura, and S. Kawata, "Three-dimensional microfabrication with two-photon-absorbed photopolymerization," Opt. Lett. **2**, 132 – 134 (1997).
6. S. Kawata, H.-B. Sun, T. Tanaka, and K. Takada, "Finer features for functional microdevices," Nature **412**, 697–698 (2001).
7. P. Danilevicius, S. Rekstyte, E. Balciunas, A. Kraniauskas, R. Jarasiene, R. Sirmenis, D. Baltriukiene, V. Bukelskiene, R. Gadonas, and M. Malinauskas, "Micro-structured polymer scaffolds fabricated by direct laser writing for tissue engineering," J. Biomed. Optics **17**, 081405 (2012).

#190823 - $15.00 USD Received 20 May 2013; revised 29 Jul 2013; accepted 29 Aug 2013; published 18 Sep 2013

8. M. Malinauskas, A. Žukauskas, G. Bičkauskaitė, R. Gadonas, and S. Juodkazis, "Mechanisms of three-dimensional structuring of photo-polymers by tightly focussed femtosecond laser pulses," Opt. Express **18**, 10209–10221 (2010).
9. K. K. Seet, S. Juodkazis, V. Jarutis, and H. Misawa, "Feature-size reduction of photopolymerized structures by femtosecond optical curing of SU-8," Appl. Phys. Lett. **89**, 024106 (2006).
10. M. Farsari and B. Chichkov, "Materials processing: Two-photon fabrication," Nature Photon. **3**, 450 – 452 (2009).
11. A. Ovsianikov, J. Viertl, B. Chichkov, M. Oubaha, B. MacCraith, I. Sakellari, A. Giakoumaki, D.Gray, M. Vamvakaki, M. Farsari, and C. Fotakis, "Ultra-low shrinkage hybrid photosensitive material for multi-photon polymerization microfabrication," ACS Nano **2**, 2257–2262 (2008).
12. J.F. Xing, X.Z. Dong, W.Q. Chen, X.-M. Duan, N. Takeyasu, T. Tanaka, and S. Kawata, "Improving spatial resolution of two-photon microfabrication by using photoinitiator with high initiating efficiency," Appl. Phys. Lett. **90**, 131106 (2007).
13. Q. Wu, Y. Ma, R. Fang, Y. Liao, Q. Yu, X. Chen, and K. Wang, "Femtosecond laser-induced periodic surface structure on diamond film," Appl. Phys. Lett. **82**, 1703 (2003).
14. N. Yasumaru, K. Miyazaki, and J. Kiuchi, "Femtosecond-laser-induced nanostructure formed on hard thin films of TiN and DLC," Appl. Phys. A **76**, 983–985 (2003).
15. A. Borowiec and H. Haugen, "Subwavelength ripple formation on the surfaces of compound semiconductors irradiated with femtosecond laser pulses," Appl. Phys. Lett. **82**, 4462 (2003).
16. S. Sakabe, M. Hashida, S. Tokita, S. Namba, and K. Okamuro, "Mechanism for self-formation of periodic grating structures on metal surface by femtosecond laser pulse," Phys. Rev. B **79**, 033409 (2009).
17. M. Hashida, Y. Ikuta, Y. Miyasaka, S. Tokita, and S. Sakabe, "Simple formula for the interspaces of periodic grating structures selforganized on metal surfaces by femtosecond laser ablation," Appl. Phys. Lett. **102**, 174106 (2013).
18. Y. Shimotsuma, P. Kazansky, J. Qiu, and K. Hirao, "Self-organized nanogratings in glass irradiated by ultrashort light pulses," Phys. Review Lett. **91**, 247405 (2003).
19. P. Rajeev, M. Gertsvolf, E. Simova, C. Hnatovsky, R. Taylor, V. Bhardwaj, D. Rayner, and P. Corkum, "Memory in nonlinear ionization of transparent solids," Phys. Rev. Lett. **97**, 253001 (2006).
20. M. Birnbaum, "Semiconductor surface damage produced by ruby lasers," J. Appl. Phys. **36**, 3688 (1965).
21. A. Ovsianikov, J. Viertl, B. Chichkov, M. Oubaha, B. MacCraith, I. Sakellari, A. Giakoumaki, D. Gray, M. Vamvakaki, M. Farsari, and C. Fotakis, "Ultra-low shrinkage hybrid photosensitive material for two-photon polymerization microfabrication," ACS Nano **2**, 2257–2262 (2008).
22. A. Ovsianikov, M. Malinauskas, S. Schlie, B. Chichkov, S. Gittard, R. Narayan, M. Löbler, K. Sternberg, K.-P. Schmitz, and A. Haverich, "Three-dimensional laser micro- and nano-structuring of acrylated poly(ethylene glycol) materials and evaluation of their cytoxicity for tissue engineering applications," Acta Biomater. **7**, 967–974 (2011).
23. 3DPoli@gmail.com.
24. M. Malinauskas, V. Purlys, M. Rutkauskas, A. Gaidukevičiutė, and R. Gadonas, "Femtosecond visible light induced two-photon photopolymerization for 3D micro/nanostructuring in photoresists and photopolymers," Lith. J. Phys. **50**, 201–208 (2010).
25. E. G. Gamaly, *Femtosecond Laser-Matter Interactions: Theory, Experiments and Applications* (Pan Stanford Publishing, USA, 2011).
26. S. Juodkazis, A. V. Rode, E. G. Gamaly, S. Matsuo, and H. Misawa, "Recording and reading of three-dimensional optical memory in glasses," Appl. Phys. B **77**, 361–368 (2003).
27. J. Sipe, J. Young, J. Preston, and H. Van Driel, "Laser-induced periodic surface structure. I. Theory," Phys. Rev. B **27**, 1141–1154 (1983).
28. R. Buividas, T. Kudrius, R. Sliupas, L. Rosa, G. Slekys, S. Bagdonas, R. Rotomskis, and S. Juodkazis, "Ripple-patterned substrates for light enhancement applications," Proc. SPIE **7376**, 737620 (2010).
29. R. A. Ganeev, M. Baba, T. Ozaki, and H. Kuroda, "Long- and short-period nanostructure formation on semiconductor surfaces at different ambient conditions," J. Opt. Soc. Am. B **27**, 1077–1082 (2010).
30. R.Buividas, L. Rosa, R. Šliupas, T. Kudrius, G. Šlekys, V. Datsyuk, and S. Juodkazis, "Mechanism of fine ripple formation on surfaces of (semi)transparent materials via a half-wavelength cavity feedback," Nanotechnology **22**, 055304 (2011).
31. L. P. R. Ramirez, M. Heinrich, S. Richter, F. Dreisow, R. Keil, A. V. Korovin, U. Peschel, S. Nolte, and A. Tünnermann, "Tuning the structural properties of femtosecond-laser-induced nanogratings," Appl. Phys. A **100**, 1–6 (2010).
32. F. Liang, R. Vallee, and S. L. Chin, "Mechanism of nanograting formation on the surface of fused silica," Opt. Express **20**, 4389–4396 (2012).
33. L. Bressel, D. de Ligny, C. Sonneville, V. Martinez, V. Mizeikis, R. Buividas, and S. Juodkazis, "Femtosecond laser induced density changes in GeO_2 and SiO_2 glasses: fictive temperature effect [Invited]," Opt. Mat. Express **1**, 605 (2011).
34. B. Wu, M. Zhou, J. Li, X. Ye, G. Li, and L. Cai, "Superhydrophobic surfaces fabricated by microstructuring of stainless steel using a femtosecond laser," Appl. Surf. Science **256**, 61–66 (2009).

#190823 - $15.00 USD Received 20 May 2013; revised 29 Jul 2013; accepted 29 Aug 2013; published 18 Sep 2013

35. R. Buividas, P. R. Stoddart, and S. Juodkazis, "Laser fabricated ripple substrates for surface-enahnced Raman scattering," Annalen der Physik **524**, L5 – L10 (2012).
36. Y. Liao, Y. L. Shen, L. L. Qiao, D. P. Chen, Y. Cheng, K. Sugioka, and K. Midorikawa, "Femtosecond laser nanostructuring in porous glass with sub-50 nm feature sizes," Opt. Lett. **38**, 187 – 189 (2013).
37. C. Hnatovsky, V. Shvedov, W. Krolikowski, and A. Rode, "Revealing local field structure of focused ultrashort pulses," Phys. Rev. Lett. **12**, 123901 (2011).
38. R. Taylor, C. Hnatovsky, E. Simova, P. Rajeev, D. Rayner, and P. Corkum, "Femtosecond laser erasing and rewriting of self-organized planar nanocracks in fused silica glass," Opt. Lett. **32**, 2888–2890 (2007).
39. R. Taylor, E. Simova, and C. Hnatovsky, "Creation of chiral structures inside fused silica glass," Opt. Lett. **33**, 1312–1314 (2008).
40. K. Ueno, S. Juodkazis, T. Shibuya, V. Mizeikis, Y. Yokota, and H. Misawa, "Nano-particle-enhanced photopolymerization," J. Phys. Chem. C **113**, 11720–11724 (2009).
41. J. Morikawa, E. Hayakawa, T. Hashimoto, R. Buividas, and S. Juodkazis, "Thermal imaging of a heat transport in regions structured by femtosecond laser," Opt. Express **19**, 20542–20550 (2011).
42. J. Morikawa, A. Orie, T. Hashimoto, and S. Juodkazis, "Thermal and optical properties of the femtosecond-laser-structured and stress-induced birefringent regions of sapphire," Opt. Express **18**, 8300–8310 (2010).
43. J. Morikawa, A. Orie, T. Hashimoto, and S. Juodkazis, "Thermal diffusivity in femtosecond-laser-structured micro-volumes of polymers," Appl. Phys. A. **98**, 551–556 (2010).
44. J. Morikawa, A. Orie, T. Hashimoto, and S. Juodkazis, "Thermal and optical properties of femtosecond laser-structured PMMA," Appl. Phys. A **101**, 27–31 (2010).
45. S. Rekštyte, M. Malinauskas, and S. Juodkazis, "Three-dimensional laser micro-sculpturing of silicone: towards bio-compatible scaffolds," Opt. Express **21**, 17028 (2013).
46. S. Maruo, T. Hasegawa, and N. Yoshimura, "Single-anchor support and supercritical CO_2 drying enable high-precision microfabrication of three-dimensional structures," Opt. Express **17**, 20945 – 20951 (2009).
47. T. Kondo, S. Juodkazis, and H. Misawa, "Reduction of capillary force for high-aspect ratio nanofabrication," Appl. Phys. A **81**, 1583 – 1586 (2005).
48. M. Malinauskas, A. Zukauskas, V. Purlys, K. Belazaras, A. Momot, D. Paipulas, R. Gadonas, A. Piskarskas, H. Gilbergs, A. Gaidukeviciute, I. Sakellari, M. Farsari, and S. Juodkazis, "Femtosecond laser polymerization of hybrid/integrated micro-optical elements and their characterization," J. Opt. **12**, 124010 (2010).
49. C. Coenjarts and C. Ober, "Two-photon three-dimensional microfabrication of poly(dimethylsiloxane) elastomers," Chem. Mater. **16**, 5556–5558 (2004).
50. M. Malinauskas, D. Baltriukiene, A. Kraniauskas, P. Danilevicius, R. Jarasiene, R. Sirmenis, A. Zukauskas, E. Balciunas, V. Purlys, R. Gadonas, V. Bukelskiene, V. Sirvydis, and A. Piskarskas, "In vitro and in vivo biocompatibility study on laser 3D microstructurable polymers." Appl. Phys. A **108**, 751–759 (2012).
51. R. Houbertz, G. Domann, J. Schulz, B. Olsowski, L. Frohlich and W.-S. Kim, "Impact of photoinitiators on the photopolymerization and the optical properties of inorganicorganic hybrid polymers," Appl. Phys. Lett. **84**, 1105–1107 (2004).
52. S. Juodkazis, V. Mizeikis, K. K. Seet, H. Misawa, and U. G. K. Wegst, "Mechanical properties and tuning of three-dimensional polymeric photonic crystals," Appl. Phys. Lett. **91**, 241904 (2007).
53. K. Cicha, T. Koch, J. Torgersen, Z. Li, R. Liska, and J. Stampfl, "Youngs modulus measurement of two-photon polymerized micro-cantilevers by using nanoindentation equipment," J. Appl. Phys. **112**, 094906 (2012).

1. Introduction

Direct laser writing with ultra-short sub-1 ps laser pulses can reach resolution of 100 nm in all three dimensions (3D) which is below the diffraction limit and enters space of nanotechnology. Recent in-bulk 3D structuring of photo-polymers showed that various photo-materials can be 3D structured with high resolution close to the light wavelength $\propto \lambda_0$ at tight focusing conditions ($NA > 1$) with a pulse durations ranging from nanoseconds to femtoseconds and even a continuous wave illumination can be used for 3D photonic crystal fabrication [1–4]. Moreover, despite the pulse duration t_p changing over incredible 6 orders of magnitude in the case of pulsed irradiation, the pulse energy E_p and the exposure dose is usually within the same order of magnitude [3, 4]. The 3D structuring initially branded as two-photon polymerization [5, 6] now can be achieved via a controlled thermal and avalanche absorption (both are linear processes) at well controlled exposure conditions. The exposure doses used in 3D structuring of polymers are in the range of a therapeutic and not in a surgery regime of live tissue [7], which makes 3D structuring appealing for biologic and medical applications.

Better understanding of 3D laser structuring is still required since changes of the pulse dura-

#190823 - $15.00 USD Received 20 May 2013; revised 29 Jul 2013; accepted 29 Aug 2013; published 18 Sep 2013

tion over several orders of magnitude in polymerization is not compatible with the multi-photon ionization, however, could be explained by domination of avalanche processes in bond breaking and polymerization [4, 8]. Indeed, it was already demonstrated that even one photon absorption at tight focusing can deliver 3D polymerization [1]. Also, a direct plasma emission (a black body radiation) into the absorption band of polymers at 2-3 μm window was consistent with size scaling of polymerized 3D structures in SU-8 using fs-laser irradiation [9]. With an increasing popularity of sol-gel resists, photo-initiators can be easily chosen and mixed with resist for tests of polymerization mechanisms by fs-laser pulses [10, 11]. It was shown that the highest resolution of 3D structuring is achieved in pure organic-inorganic SZ2080 resist without photo-initiator [8] believed to be essential for a nonlinear absorption [12].

Surface laser structuring of dielectrics [13–15] and metals [16, 17] by ablation and formation of ripples (called also light-induced periodic surface structures) using fs-laser pulses is another active area of research where mechanisms are strongly debated. On surface of metals ripples with sub-wavelength periods are formed apparently via parametric generation of a surface plasmon polariton (SPP) with a back reflection of a scattered wave at a shifted frequency; the energy and momentum conservation reads: $\omega_l = \omega_2 + \omega_{SPP}$ and $\mathbf{k}_l = \mathbf{k}_2 + \mathbf{k}_{SPP}$, where ω_l and $\mathbf{k}_l$ are the cyclic frequency and wavevector of the laser wave, subscript 2 is for the scattered color-shifted wave, and SPP is for the surface wave. Moreover, ripples can be formed inside materials [18] – the bulk-ripples – and on the surface with periods dependent on irradiation conditions and material properties (molten flows and instabilities are affecting the final morphology). Since ripples are formed at high electron density of a pre-breakdown and breakdown plasma [19], avalanche processes are essential; we present analysis of avalanche role in surface (ripples) and bulk (polymerization) structuring with ultra-short laser pulses.

Here we show how a controlled avalanche ionisation driven by ultra-short laser pulses can be used for a sub-diffraction-limited structuring by ablation on surfaces and how the laser polymerization can be achieved without use of photo-initiators. Via controlled light interaction with a free electron plasma the dielectric breakdown can be localized within a sub-100 nm cross-section on sapphire surface and polymerization via the electron avalanche can deliver 3D cure of photo-polymers.

2. Experimental

2.1. Ripples on the surface of sapphire

Ripples [20] on a 400-μm-thick high purity optical grade sapphire were fabricated using an amplified Ti:Sapphire fs-laser system (Spitfire, Spectra Physics Inc.) operating at $\nu = 1$ kHz repetition rate with a pulse duration $t_p = 150$ fs. Second harmonic wavelength at 400 nm was used for surface structuring. Linearly polarized beam was focused on the front surface of sapphire using high numerical aperture $NA = 0.7$ objective (Mitutoyo Ltd.). Aerotech linear stages positioned the sample with respect to a stationary focal spot.

Set of 30 μm length lines were fabricated at different pulse energies ranging from 23.5 nJ to 45 nJ (after the objective lens) and at different scan speeds (v_{scan}) in the range 0.7 to 70 μm/s. Distance between pulses $d_{pp} = v_{scan}/\nu$ ranged from 0.7 to 70 nm and pulse-to-pulse overlap $pp = d_{foc}/d_{pp}$ ranged from 1000 to 10 pulses per focal spot, respectively; $d_{foc} = 1.22\lambda/NA = 0.7$ μm is the diameter of the focal spot. Beam was not blanked during acceleration, causing a higher pulse overlap and dose at the ends of lines due to acceleration or deceleration. Figure 1 illustrates geometry of experiments and the mechanism of ripple formation via a sphere-to-plane ionisation growth (a) similar as in the bulk of dielectrics [19] (see discussion in Sec. 4).

#190823 - $15.00 USD Received 20 May 2013; revised 29 Jul 2013; accepted 29 Aug 2013; published 18 Sep 2013

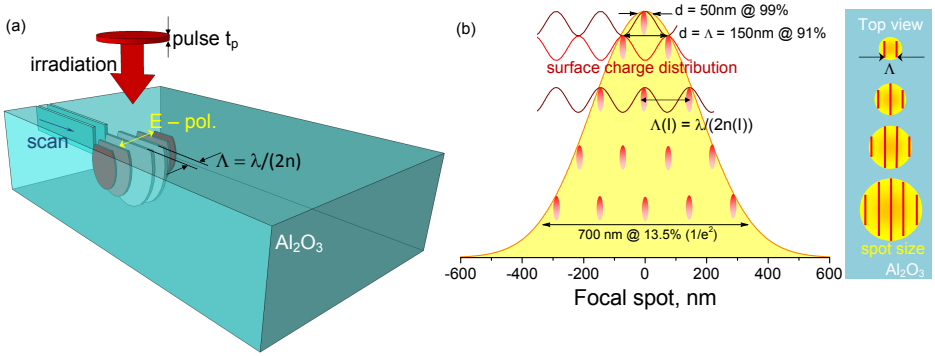

Fig. 1. (a) Plasma breakdown driven by an avalanche in a sub-surface region of a sapphire substrate under tight $NA \simeq 0.7$ focusing. Plasma nano-planes (perpendicular to the laser polarization) are formed in the bulk under the laser irradiation area and grow towards the surface (an incoming beam). (b) Geometry of interaction between subsurface scattered field superimposed with the Gaussian intensity distribution, which was used for focusing. Locations where breakdown plasma are formed marked by ellipsis. Intensity range corresponding to 50 nm diameter groove fabrication by ripple formation (>91 %) and by regular ablation (>99 %) are indicated. The period of surface charge is dependent on the free electron density, n_e, which depends on light intensity, I. Top-view projection and the spot size at different intensity cross sections with ripples shown on the right-side (see Sec. 4 for discussion).

2.2. *3D polymerization via avalanche (the one-photon process)*

We used organic-inorganic Zr containing SZ2080 (IESL-FORTH) [21] hybrid and polydimethylsiloxane (PDMS: Sylgard 184, Dow Corning) polymers as received, without adding any photo- or thermo-initiators. This allows production of 3D microstructures free from an undesired light absorbtion and cytotoxic ingredients [22]. Samples were prepared by a drop casting of resin on a standard 150-μm-thick cover glass. Prebake at 75°C for 45 min was applied for the SZ2080 sol-gel resist. After laser irradiation, SZ2080 and PDMS samples were submerged into a 4-methyl-2-pentanon bath for 30 min to develop the fabricated structures. Either no metal coating or a 10 nm of Ag was used for structural inspection by the scanning electron microscope (SEM: Hitachi TM-1000).

A 3D polymerization was carried out using fs-laser (Pharos, Light Conversion) delivering 300 fs duration pulses at a 200 kHz repetition rate. Both, fundamental 1030 nm and second harmonic 515 nm irradiation were used for SZ2080 fabrication, while for PDMS was structured at 515 nm wavelength. Objectives with different numerical apertures ($NA = 0.95, 1.25, 1.4$) were employed for beam focussing and are specified where applies. The polymerization trajectory was controlled using xy-galvanometric scanners (SCANLAB hurrySCAN II 10) and a sample positioning system Aerotech ALS130-100 (x,y-axes) with ALS130-50 (z-axis) linear motion stages ensuring a $\sim$10 nm positioning precision. A 3DPoli software was used for the control and automation of sample processing [23]. Detailed description of the setup can be found elsewhere [24].

#190823 - $15.00 USD Received 20 May 2013; revised 29 Jul 2013; accepted 29 Aug 2013; published 18 Sep 2013

3. Estimation of ionisation rates

The multi-photon absorption and avalanche rates of electron multiplication w_{mpi} and w_{imp}, respectively, are given by [25]:

$$w_{mpi} \simeq w n_{ph}^{3/2} \left(\frac{\varepsilon_{osc}}{2\Delta E} \right)^{n_{ph}}, \tag{1}$$

$$w_{imp} \simeq \frac{\varepsilon_{osc}}{\Delta E} \frac{2\omega^2 \nu_{e-ph}}{\left(\nu_{e-ph}^2 + \omega^2 \right)}, \tag{2}$$

where $n_{ph} = \Delta E e/(h\omega) + 1$ is the number of photons required for direct absorption (truncated to an integer) with ΔE being the band-gap of material, h is the Plank's constant, $\omega = 2\pi c/\lambda$ is the cyclic frequency of light of wavelength λ, e is the electron charge, and c is the speed of light. The electron quiver energy $\varepsilon_{osc} = \frac{e^2 E^2}{4m\omega^2}$ with the electrical field strength defined by intensity/irradiance, I_p, as $E = \sqrt{I_p/(c\varepsilon_0 n)}$, where ε_0 is the vacuum permittivity and n is the refractive index of the host material. The electron-ion interaction is governed by the electron-phonon momentum exchange rate $\nu_{e-ph} \simeq 6 \times 10^{14}$ s^{-1} [8]; the exact value was not critically important for this qualitative estimation of the mechanisms discussed here.

With the multi-photon absorption and avalanche rates estimated by Eqs. (1) and (2) it is possible to calculate the rate of free electron generation, hence, the rate free radicals (broken chemical bonds) are created:

$$\frac{dn_e}{dt} = n_e w_{imp} + n_a w_{mpi}, \tag{3}$$

where n_e is free electron density (available only for the avalanche multiplication) and n_a is the atom density (available only for the multi-photon ionization). Solution of the Eqs. (3) is following:

$$n_e(I,\lambda,t) = \left[n_{e0} + \frac{n_a w_{mpi}}{w_{imp}} [1 - e^{-w_{imp}t}] \right] e^{w_{imp}t} \tag{4}$$

This equation allows to follow explicitly temporal evolution of ionisation for the known temporal intensity envelope $I(t)$ [26]; here n_{e0} is the initial (dark) electron density in material $\sim 10^{10}$ cm^{-3}.

When second harmonic excitation is used, effects of long ns-background are suppressed which otherwise can significantly alter the avalanche ionization since the avalanche rate scales as $\propto \lambda^2$ (Eqs. (2)).

4. Results and Discussion

We show (i) formation of a single groove of ~ 70 nm (or $\lambda/6$) by a controlled laser ablation and (ii) 3D polymerization when a linear light-matter interaction prevails. The results are discussed in the context of the mechanisms which are active topic of research in laser micro-/nano-processing.

4.1. Ripples: towards an ultimate resolution

Since the first observation of ripples by Birnbaum in 1965 [20] they attracted a lot of attention both from the pure science and applications in sensing, optical memory, polarisation control, microfluidics and packaging. Most of ripples phenomenology can be accounted for by interaction of incident and scattered fields on the surface [27]. However, ripples on surfaces of dielectrics are less well behaved and periods in the range $\Lambda = \lambda_0/(2-20)$ have been reported especially for excitation with fs-laser pulses. Most of them scales closely to the empirical $\Lambda = \lambda_0/n/2$ where n is the refractive index of an unperturbed material [28] and dielectric

#190823 - $15.00 USD Received 20 May 2013; revised 29 Jul 2013; accepted 29 Aug 2013; published 18 Sep 2013

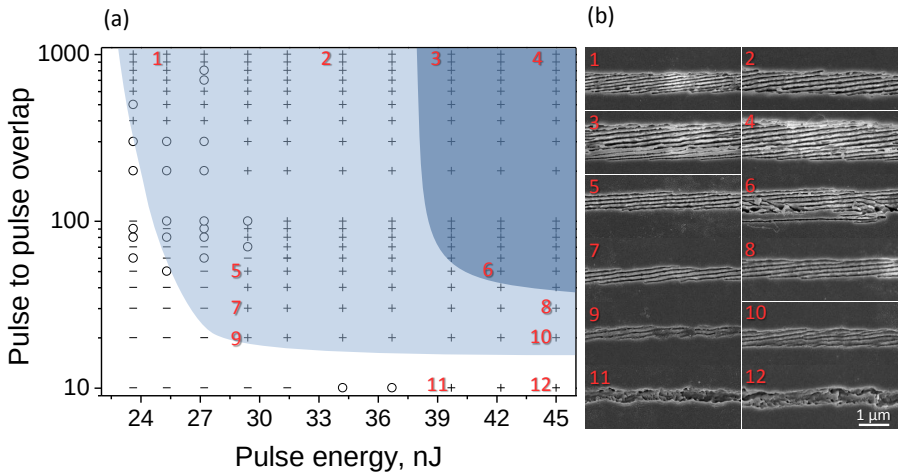

Fig. 2. (a) A parameter space for ripple formation: number of pulses per focal spot $pp = d_{foc}/d_{pp}$ vs. pulse energy E_p for 400 nm/150 fs pulses focused using $NA = 0.7$ objective lens. 30 μm long lines with parallel ripples were fabricated for each condition. A colored region indicates ripple formation region, where light-shade color indicates uniform, not damaged ripples, while darker-shade region show where ripples start to deteriorate due to increased ablation; a "+" sign indicates full line fabrication, "–" no fabrication and "○" a partial line fabrication. (b) SEM images of ripples representing different fabrication conditions, numbers link parameters with the SEM images.

permittivity of the ambient medium [29]. However, since n is dependent on intensity via strong electronic excitation during the pulse, $n(I,t_p)$, this transient permittivity can imprint ripples of different periods. Laser ablation and ripple formation can be, in fact, tuned to produce a single groove pattern as shown below.

4.1.1. Ripples on sapphire

Lines fabricated by single scan of the laser beam contain several grooves – ripples (Fig. 2(b)) which can then be patterned over larger area by scanning [28]. Ripples on surfaces of high melting temperature substrates such as sapphire and SiC showed almost intensity independent period $\lambda_0/n/2$ [28,30]. Here we study wide parameter space of the ripple formation (Fig. 2(a)) and a weak, but discernible dependence of the period on a pulse energy (Fig. 3(a)) and overlap between pulses (Fig. 3(b)) was observed. Generation of free electrons (plasma) creates a negative contribution to the refractive index $n(I) = n_0 - \Delta n$ (with $\Delta n > 0$) where changes are proportional to the electron density $\Delta n \propto n_e$, hence intensity. This should cause an increase of the ripple period $(\lambda_0/n(I))/2$, the trend observed in experiments (Fig. 3(a)). The ripple period calculated using a refractive index of unaffected sapphire, $n_0 = 1.79$, is equal to 112 nm, which is close to the measured period values at a low pulse energy and a high pulse overlap. It is important to note that period saturates at certain value ~160 nm; this is consistent with a dielectric ablation theory [25], which predicts that at the ablation threshold, the free electron number density approaches the atomic number density, hence saturates. The dependence of ripple period on energy was most pronounced for high pulse to pulse overlap, presumably because high number of pulses are required to establish the most stable conditions (e.g, accumulation of point defects in lattice and trapped charges).

Figure 3(b) shows that the smallest ripple period, close to the one predicted by unmodified refractive index of sapphire, was only obtained at the lowest pulse energy 25 nJ and above

#190823 - $15.00 USD Received 20 May 2013; revised 29 Jul 2013; accepted 29 Aug 2013; published 18 Sep 2013

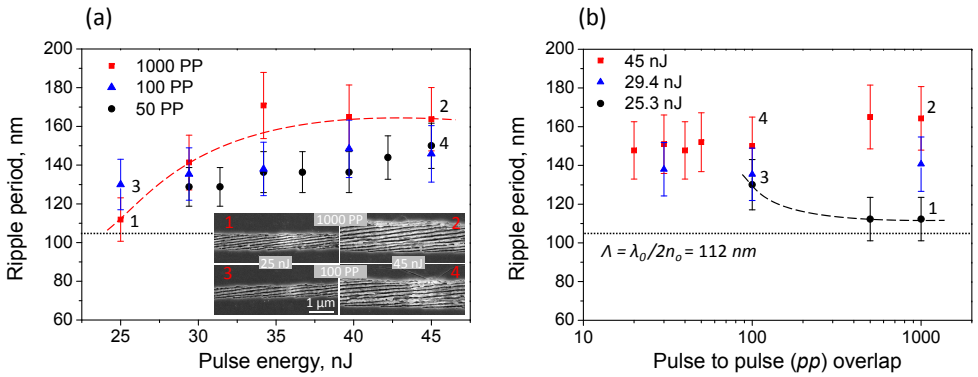

Fig. 3. (a) A ripple period dependence on a pulse energy at three different pulse-to-pulse (*pp*) overlap values: 50, 100 and 1000. At low pulse energy and high *pp* overlap, period is close to predicted by $\lambda_0/2n_0$ = 112 nm, where n_0 is refractive index for laser unaffected sapphire, value indicated on graphs by dotted line. Period is increasing with energy and saturates at ∼160 nm. Trend is more pronounced for higher *pp* values. (b) A ripple period dependence on *pp* overlap at the three different pulse energies: 25, 29 and 45 nJ. Only at the lowest energy period decreases with overlap. Inset shows SEM images linked by numbers with values on (a) and (b) graphs.

500 *pp* overlap. The dependence of ripple period on the pulse overlap was much weaker as compared to the dependence on the pulse energy. Only a minor period decrease (from 130 to 110 nm) was observed for the overlap between 100 and 500 *pp*, respectively, at the lowest energy. The full set of pulse-to-pulse overlap values ranged from 10 to 1000 *pp* and was tested at different energies from the ripple fabrication threshold to few times above it. A similar trend, reduction of the ripple period at a higher pulse overlap, was observed in the bulk [31] and on the surface [32] of a fused silica, however dependence was much stronger. To compare, on the surface of fused silica ripple period reduced about 3 times (from 260 to 80 nm) for a pulse overlap change from 20 to 500 *pp* (using 45 fs, 800 nm pulses). To explain this difference, material properties are important. Fused silica has a lower refractive index, a lower melting temperature (1600°C vs 2040°C for sapphire), has a fictive temperature anomaly, i.e., a denser phase at a higher temperature [33].

4.1.2. Single groove-ripple on sapphire

Figure 4 shows how the ripple formation can be dynamically tuned to a single-groove ablation as exposure dose becomes close to the threshold (by changing the pulse overlap). Figure 1(b) schematically depicts the number of ripple periods $\Lambda \simeq 150$ nm, which fit into the focal spot at a different intensity cross sections; here the Gaussian intensity profile of 700 nm diameter at a $1/e^2$ intensity level is shown, which is the same as used for the fabrication: $d_{foc} = 1.22\lambda/NA =$ 700 nm. Both parameters, the pulse overlap and energy have to be optimised for a single groove formation. At the beginning of line scan where overlap of pulses occurs, an initiation of ripple formation was observed. Then, a single groove (ripple) can be made by reducing the overlap or energy of laser pulses. Higher overlap creates more ripples, because preceding pulses creates defects and reduces the ablation threshold, so lower intensity regions of Gaussian distribution can to interact with material and so increase fabrication line width. Assuming the Gaussian intensity envelope, it was estimated that a single groove can be formed, if the maximum pulse intensity is less than ∼10 % above the ablation threshold. Tere, beam width is below 150 nm and two-grooves cannot fit into the spot. It is not difficult to achieve a 10 % pulse energy stability

#190823 - $15.00 USD Received 20 May 2013; revised 29 Jul 2013; accepted 29 Aug 2013; published 18 Sep 2013

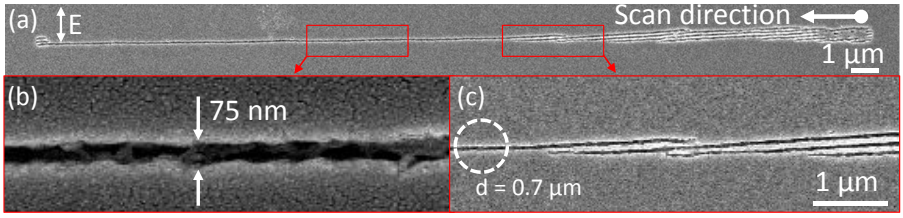

Fig. 4. Ripples fabricated on a sapphire substrate by 25 nJ / 150 fs laser pulses at 400 nm wavelength and 500 *pp* overlap, beam focused using $NA = 0.7$ objective lens. Sample was scanned at 14 μm/s speed, beam was not blanked during acceleration. (a) 30 μm length line consisting of different number of ripples and extended length of a single ripple. Zoomed-in section (b) show groove width (50-75 nm), (c) transition from 3 to 2 to 1 ripple / groove, diameter of the focal spot (0.7 μm) indicated by circle.

with current fs-lasers to control such process. In this regime a single groove of a 50 - 70 nm diameter is formed. To compare the intensity stability required to achieve a 50 nm diameter groove without ripple formation effect, stability close to 1 % (the Gaussian beam intensity is at a 99 % level at 50 nm diameter) would be required as shown in Fig. 1(b). We demonstrate here, that ripple fabrication is more than a technique for the uniform surface nano-texturing, which has already found many applications, e.g., for surface wettability control [34] and as surface-enhanced Raman (SERS) substrates [35], but it is also promising as the highest resolution direct laser writing technique.

A single groove has been demonstrated in the case of in-bulk ripples in porous glasses [36] with a single nano-plane crack formed at a close-to-critical irradiance. We show here that a single sub-100-nm-wide groove is recorded on the surface on sapphire (Fig. 4). The dielectric breakdown of the surface can be scanned over the surface making the pattern of a very high resolution $res = width/(1.22\lambda_0/NA) \simeq 70$ nm$/700$ nm $\simeq 10$ (one tenth of the diffraction limit at the employed focusing). Hence, similarly to the inscription of radial and azimuthal polarizations [37], the linear polarization can be imprinted as a single sub-diffraction groove.

This observation is consistent with formation of ripples starting in a sub-surface region via plasma sphere-to-plane formation since the sub-critical plasma density is required and it grow towards the surface where it is imprinted by ablation (Fig. 1(a)). The self-organization and quasi-periodicity of ripples occurs via self-organization and pairing of the plasma planes $(\lambda_0/n)/2$ [30] (Fig. 1(b)). Crests of the wave are locations of augmented electron density where the breakdown occurs. Accumulation of the light-induced defects is important for the ripple formation and can be rationalized via a stochastic seeding of the defects where subsequent pulses start ionisation, which evolves into the planes. This mechanism is consistent with formation of the bulk ripples [38, 39].

4.1.3. Hysteresis in ripple formation

Finally, an interesting behavior of the ripple formation threshold with orientation parallel ($\parallel$) or perpendicular ($\perp$) to the scan was observed (Fig. 5). There is approximately a 10% difference in the pulse energy threshold and the periods slightly differs $\Lambda_\perp < \Lambda_\parallel$. Apparently, the plasma density created for the $\parallel$-ripples is larger than that for $\perp$ ones. Larger plasma density is expected from the regions where larger number of structural defects is accumulated, material is preheated, amorphous or noncrystalline regions are created on a crystalline substrate [28]. In all of those situations stronger absorption is expected. As pattern of ripples develops, it has nano-features or roughness down to tens of nanometers [35].

#190823 - $15.00 USD Received 20 May 2013; revised 29 Jul 2013; accepted 29 Aug 2013; published 18 Sep 2013

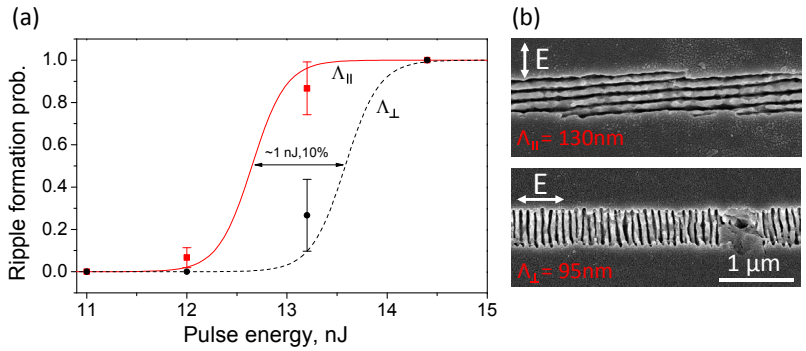

Fig. 5. (a) Probability of the ripple formation at different energies for the parallel ($\parallel$ to the fabrication line) and perpendicular ($\perp$) ripples. Threshold is about 10 % lower for the parallel ripples. Each dot on the graph was calculated as an average probability from 3 trials; 10 lines were fabricated in each trial. (b) SEM images of the typical $\parallel$- and $\perp$-ripples. Polarization direction and ripple period are indicated.

Anisotropy of temperature diffusivity induced by ripples is important and discussed next. The $\parallel$-ripples facilitate thermal transport along the scan direction and the heat affected zone is expected to advance further along scan as compared with the $\perp$-ripples. As a result creation of defects, amorphous regions, etc., is favored in the case of $\parallel$-ripples. This is why plasma density n_e is expected to be larger in this case and correspondingly the larger period $\Lambda_{\parallel} = \lambda/(n_0 - \Delta n(n_e))/2$ is observed.

We have shown earlier by polymerization [40] that nano-structures and nanoparticles can localize temperature and the nano-structured regions are hot for longer since the mean free path of heat carriers (electrons and phonons), $l_{mfp} = v_t\tau$ becomes smaller, here v_t is the thermal velocity of heat carriers, τ is the time between scattering events. This causes a decrease of the thermal conductivity $\chi = \rho v_t c l_{mfp}/3$, where c is the specific heat, ρ is the density of carriers. Temperature localization due to decrease of temperature diffusivity by 1-2% in the fs-laser structured regions of polymers and sapphire has been demonstrated by direct measurements [41–44]. In those cases, a laser structuring inside the bulk was made at the conditions when bulk-ripples are not formed.

Further studies are required to explore surface plasma formation on dielectrics which create conditions of parametric generation of surface structures similar to the reported in metals [16], where period dependence on pulse energy scales in a similar fashion as shown in Fig. 3(a). In metals ripples with periods corresponding to the surface plasma wave with energy $\omega_p/\sqrt{2}$ (ω_p is the plasma density) are imprinted on surfaces at the dielectric breakdown conditions when the critical plasma density is ω_{cr}; the ripple period is $\Lambda \simeq \frac{2}{3}\lambda \propto (\omega_{cr}/\sqrt{2})^{-1} \approx (\frac{3}{2}\omega_{cr})^{-1}$ [16].

4.2. 3D polymerization: structuring without photo-initiators

We show here 3D polymerization when photo-initiators are not used and estimate ionisation rates according to formulae given in Sec. 3 at different wavelengths and exposure conditions. The detailed experimental conditions are presented in refs. [8, 45].

The SZ2080 resist without a two-photon absorbing initiator can be 3D structured with high resolution and good structural quality by fs-laser pulses [8]. The avalanche rate is several orders of magnitude higher as compared with the multi-photon (4-photon) ionisation in the case of $\lambda_l = 1030$ nm fs-laser pulses. Photonic crystal structures with log's lateral cross section $d \simeq$ 300 nm were fabricated at 1030 nm wavelength and retrieved after a wet-bath development

#190823 - $15.00 USD Received 20 May 2013; revised 29 Jul 2013; accepted 29 Aug 2013; published 18 Sep 2013

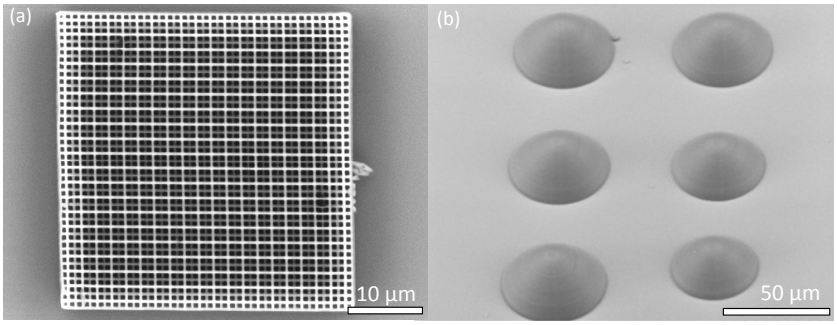

Fig. 6. 3D functional microstructures produced in a SZ2080 resist without a photo-initiator: (a) photonic crystal fabricated using 1 kHz pulse repetition rate, 1030 nm wavelength, $NA = 1.4$ focusing and 16.5 nJ pulse energy. (b) An array of microlenses fabricated using 200 kHz pulse repetition rate, 515 nm wavelength, $NA = 0.95$ focusing, 1.1 nJ pulse energy (0.22 mW) and 0.1 mm/s sample translation velocity.

(Fig. 6(a)). Resolution can be improved by up to 40% using a critical point dryer [46] which prevents a capillary collapse [47].

Two-photon absorption of SZ2080 (without a photo-initiator) at the second harmonic $\lambda_l =$ 515 nm irradiation is expected to be efficient due to $\lambda_l = 0.7\lambda_g$ [8] (λ_g is the wavelength of direct absorption). However, at the employed high intensities the avalanche prevailed in 3D polymerization of structures shown in Fig. 6(b); see estimations in Sec. 4.3. Polymerization of SZ2080 was performed without use of photo-initiators at 1030 and 515 nm wavelength irradiation. Pulse energy, required for polimerisation was only $\sim$10 times different, while a larger difference is expected for the nonlinear absorption. To expedite fabrication of micro-optical elements over large areas with sub-1 mm cross sections we use a surface contour definition by laser writing [48], then development, and subsequent uniform UV exposure. This delivers up to a 100 times faster fabrication of simple shapes of micro-optical elements such as lenses and prisms [48].

Laser structuring of bio-compatible polymers with laser direct write is expected to find wide field of applications [45]. Scaffolds can be formed in pure SZ2080 (Fig. 7(a)) which are bio-incompatible due to absence of photo-initiators. PDMS was also laser structured without use a photo-initiator at throughput higher as reported earlier [49] (see, Fig. 7(b)). Efficient fabrication is required for practical bio-medical applications [7, 22, 50]. We found (Table 1) that avalanche is much more efficient in ionisation and bond opening, which is required for cross-linking of PDMS as compared with a 3-photon ionisation at the used 515 nm irradiation (for rate comparison see Sec. 4.3).

Table 1. Ionisation rates estimated by formulae in Sec. 3 for the used fabrication conditions.

λ, nm	Material	λ_g, nm	$I_p \times 10^{13}$, W/cm^2	$w_{mpi} \times 10^{10}$, s^{-1}	$w_{imp} \times 10^{13}$, s^{-1}
400	Sapphire	150	6.11	10.49	3.84
515	PDMS	225	0.34	0.04	0.64
515	SZ2080	325	0.17	3.70	0.44
1030	SZ2080	325	0.87	3.40	8.40

#190823 - $15.00 USD Received 20 May 2013; revised 29 Jul 2013; accepted 29 Aug 2013; published 18 Sep 2013

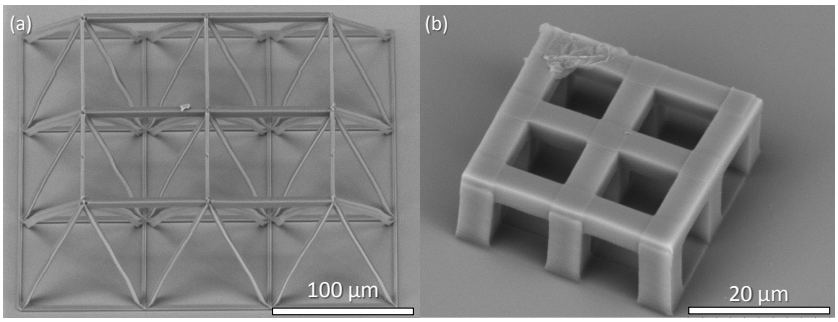

Fig. 7. 3D structures produced in SZ2080 and PDMS without photo-initiators at 515 nm, 200 kHz irradiation: (a) array of pyramids fabricated in SZ2080 using $NA = 0.95$ focusing, 1.75 nJ pulse energy (0.35 mW) and a 0.2 mm/s sample translation velocity. (b) Bioscaffold fabricated in PDMS using $NA = 1.25$ focusing, 2.5 nJ (0.5 mW), 2 nJ (0.4 mW) and 1.5 nJ (0.3 mW) pulse energies for the upper layer, supporting pillars and the secondary scan, respectively and 0.1 mm/s sample translation velocity.

4.3. Estimation of multi-photon and avalanche rates

Let us evaluate the values of w_{mpi} and w_{imp} for the used polymerization of undoped PDMS, SZ2080 and in the case of ripple formation on sapphire. For PDMS, a strong absorption starts at $\lambda_g \simeq 225$ nm or $J_i = 5.5$ eV and is considered as a direct absorption transition; in case of SZ2080 $\lambda_g \simeq 325$ nm and $\lambda_g \simeq 150$ nm for sapphire.

Estimation of the ionization rates are given next for the typical conditions used in experiments. Surface of sapphire was laser textured by ripples with $E_p = 35$ nJ which corresponds to an average irradiance of $I_p = E_p/(\pi w_0^2 t_p) \simeq 6.11 \times 10^{13}$ W/cm^2 for the 3-photon process. The ionisation rates one can find directly from Eqs. (1)–(2): for multi-photon $w_{mpi} \simeq 10.49 \times 10^{10}$ s^{-1} and $w_{imp} \simeq 3.84 \times 10^{13}$ s^{-1} for avalanche; refractive index $n = 1.7$.

In PDMS for the typical $E_p = 2$ nJ at $NA = 1.25$ focusing the avalanche is even more efficient as compared with sapphire $w_{mpi} \simeq 3.9 \times 10^8$ s^{-1} and $w_{imp} \simeq 6.4 \times 10^{12}$ s^{-1}; refractive index $n = 1.4$. In the most narrow bandgap material SZ2080 at the laser wavelength $\lambda_0 = 515$ nm, the ionisation by a two-photon process $n_{ph} = 2$ is expected according to the favorable $\lambda_l = 0.7\lambda_g$ [8] conditions; refractive index $n = 1.45$. For the highest resolution structures in SZ2080 obtained with $NA = 1.4$ objective lens and $E_p = 16.5$ nJ, the intensity $I_p \simeq 8.7 \times 10^{12}$ W/cm^2 (for 4-photon process at 1030 nm). Correspondingly, the rates are: $w_{mpi} \simeq 3.4 \times 10^{10}$ s^{-1} and $w_{imp} \simeq 8.4 \times 10^{13}$ s^{-1} (Fig. 6(a)). At the 515 nm when two-photon can be efficient and for $E_p = 1.75$ nJ (Fig. 7(a)) the difference between the two ionisation mechanisms becomes slightly smaller: $w_{mpi} \simeq 3.7 \times 10^{10}$ s^{-1} and $w_{imp} \simeq 4.4 \times 10^{12}$ s^{-1}.

In all the analysed cases the avalanche is a prevailing ionisation mechanism up to the dielectric breakdown when $\nu_{e-ph} \simeq c/\lambda$ (see, Table 1).

5. Conclusions

We show that avalanche ionisation plays an essential role in surface nano-texturing by ripples and that it can be controlled to achieve ten times higher resolution as compared with the diffraction limit at the used $NA = 0.7$ focusing. A single 50-75 nm wide groove was fabricated using linear polarization on sapphire surface. This is an example of a controlled avalanche breakdown of the surface. Different thresholds for ripples oriented $\parallel$ and $\perp$ to the scan direction was found to be $\sim 10\%$ and can be attributed to the temperature diffusivity changes due to nano-texturing. The sphere-to-plane ionisation model can explain formation of ripples as well as the single

#190823 - $15.00 USD Received 20 May 2013; revised 29 Jul 2013; accepted 29 Aug 2013; published 18 Sep 2013

groove.

The 3D photostructuring of of SZ2080 and PDMS polymers without photoinitiators at different focussing conditions is demonstrated. Microlenses and scaffolds were produced as sample structures. This shows a potential to produce optically transparent integrated optical elements as well as bio-compatible scaffolds [50]. Though the influence of photo-initiator concentration on a polymerization rate and degree of cross linking has been investigated [51], additional studies on monomer-to-polymer conversion under the avalanche and thermal processes for 3D polymerization requires future studies as it influences mechanical [52] and biological properties [53]. Thermal black-body emission of the laser breakdown region can provide an efficient source for direct absorption into vibrational modes of some polymers [9] and enhance polymerization.

The analysed cases of surface ripple formation and 3D polymerization clearly shows an importance of avalanche via linear one-photon absorption and opens pathways for a well-controlled laser microfabrication and additive micro-manufacturing of optical elements and bio-compatible structures.

Acknowledgments

We are grateful for partial support via Discovery grants DP120102980 and DP130101205 from the Australian Research Council and Tecdia Ltd., for preparation of sapphire substrates. SR and MM acknowledges the research support by a research grant No. VP1-3.1-SMM-10-V-02-007 (Development and Utilization of a New Generation Industrial Laser Material Processing Using Ultrashort Pulse Lasers for Industrial Applications) from the European Social Fund Agency.

#190823 - $15.00 USD Received 20 May 2013; revised 29 Jul 2013; accepted 29 Aug 2013; published 18 Sep 2013